Hindawi Publishing Corporation
International Journal of Photoenergy
Volume 2012, Article ID 285129, 9 pages
doi:10.1155/2012/285129

Research Article

Preparation of Porous F-WO_3/TiO_2 Films with Visible-Light Photocatalytic Activity by Microarc Oxidation

Chung-Wei Yeh,[1] Kee-Rong Wu,[2] Chung-Hsuang Hung,[3] Hao-Cheng Chang,[2] and Chuan-Jen Hsu[4]

[1] *Department of Information System, Kao Yuan University, Kaohsiung 811, Taiwan*
[2] *Department of Marine Engineering, National Kaohsiung Marine University, Kaohsiung 811, Taiwan*
[3] *Department of Safety, Health and Environmental Engineering, National Kaohsiung First University of Science and Technology, Kaohsiung 811, Taiwan*
[4] *Metal Industries Research and Development Centre, Kaohsiung 811, Taiwan*

Correspondence should be addressed to Kee-Rong Wu, krwu@mail.nkmu.edu.tw

Received 14 July 2011; Accepted 8 September 2011

Academic Editor: Jae Sung Lee

Porous F-WO_3/TiO_2 ($mTiO_2$) films are prepared on titanium sheet substrates using microarc oxidation (MAO) technique. The X-ray diffraction patterns show that visible-light (Vis) enabling $mTiO_2$ films with a very high content of anatase TiO_2 and high loading of WO_3 are successfully synthesized at a low applied voltage of 300 V using electrolyte contenting NaF and Na_2WO_4 without subsequent heat treatment. The cross-sectional transmission electron microscopy micrograph reveals that the $mTiO_2$ films feature porous networks connected by many micron pores. The diffused reflection spectrum displays broad absorbance across the UV-Vis regions and a significant red shift in the band gap energy (~2.23 eV) for the $mTiO_2$ film. Owing to the high specific surface area from the porous microstructure, the $mTiO_2$ film shows a 61% and 50% rate increase in the photocatalytic dye degradation, as compared with the N,C-codoped TiO_2 films under UV and Vis irradiation, respectively.

1. Introduction

Titanium dioxide (TiO_2), known for being environmentally friendly and chemically stable, is one of the most suitable semiconductors for several environmental applications, including air purification, water disinfection, hazardous waste remediation, and, in recent years, the splitting of water to produce hydrogen [1–3]. Upon irradiation of photons with energies greater than or equal to the band gap energy (3.2 eV for anatase TiO_2) of the photocatalyst, the photogenerated electrons and holes can either recombine in the bulk or migrate to the surface to initiate various redox reactions. The photocatalytic (PC) reaction is usually accepted to be a surface-oriented phenomenon, regardless of whether it involves fine particles or films [1]. The surface area reportedly dominates the PC activities of the porous anodized TiO_2 oxides [4]. A high specific surface area favors PC efficiency. Hence, films that have a rough surface with a high surface area provide superior PC performance. In recent years, substantial effort has been made to improve the PC activities of TiO_2 films [4–10]. Porous TiO_2 films with a high surface area, such as porous anodized TiO_2 oxides [4], nanotube arrays [5, 6], ordered nanopore arrays [7], nanograined thin films [8], mesoporous structures [9], and hierarchical micro-/nanoporous structures [10], are of great interest for their potential to improve PC activities. Interestingly, in addition to being mechanically stable, the ordered nanopore TiO_2 arrays exhibit superior PC and photoelectrochemical (PEC) activities in the degradation of organic compounds against nanotube counterpart arrays, because of their excellent separation and the transport properties of photogenerated electron-hole pairs. In addition to having a high specific surface area, the ordered nanopore TiO_2 arrays have a network-framed structure that increases the carrier transport routes.

The use of TiO_2 is limited by its wide band gap (~3.2 eV). Semiconductors with smaller band gaps, such as

CdS (2.4 eV), Fe_2O_3 (2.3 eV), and Cu_2O (2.2 eV), commonly suffer from photocorrosion in electrolyte solution and rapid recombination of the photogenerated carriers [1]. Coupling a semiconductor with a high work function with another semiconductor can greatly enhance the oxidation of holes photogenerated in the semiconductor, by increasing the efficiency of carrier separation. Heterostructured oxides, such as TiO_2/ITO, TiO_2/WO_3, CdS/TiO_2, and TiO_2/SnO_2, have been proposed for providing a potential driving force for separating photogenerated charge carriers [2, 11–14]. Of the coupled semiconductors, ITO is the most popular transparent conductive substrates used in photoanodes and photocatalysis [2, 12], but it is one of the most expensive materials and has a detrimental effect on its PEC activity due to the increase in resistivity of the ITO substrate [15]. Among the various heterostructured oxides, TiO_2/WO_3 has been shown to have applications in photocatalysis [9, 16, 17], biophotoelectrodes [18], and anticorrosion [19]. The improved PC activity of the TiO_2/WO_3 particles has been attributed to the increased surface acidity and improved charge separation due to the proper coupling of WO_x species with TiO_2 within the nanoparticles [9, 16, 17, 20]. The adsorption affinity of reactant molecules on the surface of the TiO_2/WO_3 photocatalyst is a more important factor than the surface reaction of the photogenerated carriers in determining PC activity. The increase in the adsorption of MB solution is more likely to be associated with an increase in the surface area of the TiO_2/WO_3 particles. However, the enhancement of PC activity under visible-light (Vis) irradiation is reportedly around one tenth of that measured under ultraviolet (UV) irradiation [21].

Some researchers have shown that the introduction of fluorine (F) atoms into a photocatalytic system effectively increases the Vis PC activity of TiO_2 [22–27]. Wu and Chen presented a high Vis PC efficiency of F-doped TiO_2 particulate thin films assisted by NaF solution. They concluded that the presence of F^- ions is critical not only to the formation of particulate TiO_2 films, but also to the formation of Ti^{3+} and oxygen vacancies upon F^- ion doping, which results in a superior PC efficiency [23]. Moreover, it has been reported that the photocatalytic activity and the anatase crystallinity of porous TiO_2 films can be enhanced by adding appropriate amount of F^- ions into the electrolyte in microarc oxidation (MAO) process [26, 27].

MAO, a plasma-assisted electrochemical process, has been used to fabricate a TiO_2 surface layer by applying a positive voltage to a Ti sheet that is immersed in an electrolyte [26]. In addition to its short process duration and less-sophisticated equipments, the MAO process is reportedly a potentially good approach for preparing porous and network-structured TiO_2 films that adhere robustly to a Ti sheet substrate [26–30]. The main mechanism in MAO involves dielectric breakdown, which causes spark discharge and microarcing. Therefore, porous oxide films form on the anode surface [29]. The porous network is regarded as an open, wormlike structure on the surface of the film, with randomly orientated channels. The approach has several potential applications, mostly involving biocompatibility, such as biomimetic apatite [31], orthopedic implants with antimicrobial coatings [30, 32–34], and wear protection [35]. Recently, some related studies have addressed the degradation of dye [4, 26, 27, 36, 37] or dye-sensitized solar cells (DSSC) [38]. For instance, He et al. recently synthesized WO_3/TiO_2 composite films using pulse-MAO at an applied voltage of 400–460 V and electrolyte consisting of Na_2WO_4, NaOH, and NaF. Most recent, porous WO_3/TiO_2 films were also fabricated by DC-MAO at an applied voltage of 450 V using Na_2WO_4 and Na_3PO_4 solution as electrolyte [36]. The relatively high applied voltage of the above-mentioned processes, however, resulted in a significant increase in the content of TiO_2 rutile phase, which is well known to be photocatalytically inferior to the anatase phase in various applications [4]. This is because that applying high voltages results in not only increasing the content of rutile phase but also decreasing the amount of WO_3 loading or W dopant in the porous TiO_2 film.

One of the advantages of MAO process is the possibility of incorporating anionic and/or cationic ions into the TiO_2 layer on an inexpensive Ti substrate, by controlling the composition and concentration of the electrolyte [28–30]. However, the MAO TiO_2 film is liable to contain some free Ti elements and has large pores and a high pore density. Postalkali or heat treatments have been used to improve the morphological and intrinsic characters of MAO coatings [4, 31, 38].

In this study, porous F-TiO_2/WO_3 ($mTiO_2$) films with incorporated cationic and anionic ions were formed by an MAO process at a relatively low applied voltage using an electrolyte with a properly chosen composition. The PC properties of the as-anodized films were tested by degrading methylene blue (MB) solution under UV and Vis irradiation.

2. Experimental Procedure

2.1. Sample Preparation. Porous $mTiO_2$ were formed on Ti substrates ($25 \times 75 \times 1$ mm) using an in-house MAO system, in which the Ti sample was applied as an anode and a stainless steel container was used as a cathode. The surfaces of the Ti substrates were polished using silicon carbide paper and ultrasonically cleaned three times for 15 min each time, in 100% acetone, 100% ethanol, and distilled water. In a series of screening experiments, the electrolyte solutions were NaF (2 g/L) with Na_2WO_4 (15 g/L), and the applied voltage was 300 V. For comparison, an undoped TiO_2 film ($uTiO_2$) and an N,C-codoped TiO_2 ($nTiO_2$) films both deposited on ITO glass substrates with about the same thickness of 1.8 μm were prepared using DC magnetron sputtering system. Details of the $nTiO_2$ films, which were prepared at a low doping concentration of N and C (<2%) were presented elsewhere [39].

2.2. Sample Characterization. The crystal structures of the samples were analyzed using a high-resolution X-ray diffractometer (XRD, Rigaku ATX-E) and a Micro-PL/ Raman spectroscope (Jobin-Yvon T64000). The surface topography of each sample was determined using an atomic force microscope (AFM, SPI 3800N, Seiko). Surface morphology and chemical composition of the samples were examined by using a scanning electron microscope (SEM, JEOL

JSM-6700F) equipped with an energy dispersive X-ray spectrometer (EDS). A transmission electron microscope (TEM, Philips Tecnai 20) was employed for microstructure characterization. TEM cross-sectional specimens of the samples were prepared using a focused ion beam (FEI Quant D 200) at a voltage of 30 kV.

The TiO_2 powders from scraping the porous $mTiO_2$ film was taken to have a BET (Brunauer-Emmett-Teller) surface area measurement. The diffused reflectance of the films was measured by using a UV-vis-NIR spectrometer (Hitachi U-4100) equipped with an integration sphere. Since the Ti substrates are completely opaque and zero transmittance to the incident light, the absorption and band gap energy (E_g) of the samples were calculated using the formula stated in [36, 37, 40]. Two light sources, UV lamps ($\lambda \sim 365$ nm) and blue-light-emitting diodes (BLED, $420 < \lambda < 530$ nm), were used to provide irradiated light intensities of 2.7 and 12.5 mW/cm^2, respectively. The PC activity was evaluated using aqueous MB solution as model pollution [15]. Aqueous MB solutions without samples were also illuminated in the same manner to generate a blank value, and such a solution with samples was not irradiated, as an adsorption test.

3. Results and Discussion

3.1. Microstructural Measurements. Figure 1 presents the XRD patterns of as-anodized $mTiO_2$ sample along with the N,C-codoped TiO_2 ($nTiO_2$) and pure TiO_2 ($uTiO_2$) for comparisons. The XRD patterns of $mTiO_2$ reveal a fully dominant anatase TiO_2 phase. The peak marked by a triangle is associated with Ti, and may derive from the Ti substrate and from not well-anodized TiO_2 oxide, which is the result of random arcing by MAO [35]. Sample $mTiO_2$ also exhibits an intense diffraction peak at $2\theta = 23.67°$ of crystalline WO_3 peaks of (020) plane, as also detailed in the inset in Figure 1. A broad diffraction peak from $2\theta = 33°$ to $34.5°$ is assigned to a crystalline WO_3 phase [41]. Comparing with $uTiO_2$ in the inset of Figure 1, the diffraction (101) plane is shifted slightly toward a lower 2θ value, suggesting possible distortion of the crystal lattice of TiO_2 by the tungsten, fluorine, or/and other dopants. However, a small shift towards higher diffraction angles, due to different ion radii of Ti and W, has been observed in the XRD patterns of the anatase TiO_2 phase as W is doped on titania [37]. Sample $mTiO_2$ has a slightly broader peak at $2\theta = 25.18°$ than the $uTiO_2$, indicating the smaller crystallite size of the $mTiO_2$. These findings imply that the substitution of Ti^{4+} ions for W^{4+} in the TiO_2 lattice to form a nonstoichiometric $W_xTi_{1-x}O_2$ solid solution may have occurred in the $mTiO_2$ film [9]. In the case considered herein, the loaded WO_3 likely favors the formation of the anatase TiO_2 phase by the MAO process, which can be further studied by acquiring Raman spectra. Thus, the WO_3 phase was loaded with a noticeable content on the TiO_2 matrix. The amounts of O, Ti, and W were found to be 68.27, 25.59, and 6.14 at.%, respectively, whereas the fluorine was too small beyond the detectable limit of the EDS. Noted also that the relative high amount of tungsten oxides of which could be promoted by addition

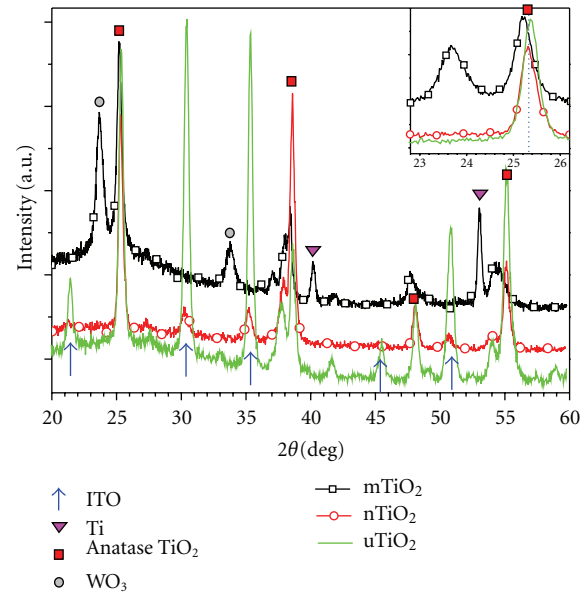

Figure 1: XRD patterns of the $mTiO_2$, $nTiO_2$, and $uTiO_2$ films.

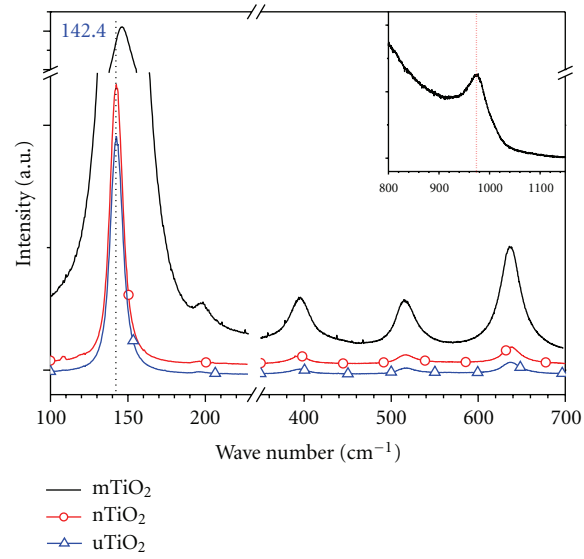

Figure 2: Raman spectra of the $mTiO_2$, $nTiO_2$, and $uTiO_2$ films.

of fluorine in the electrolyte was reportedly attributable to the high photocatalytic ability [27, 37].

Raman spectra in the range of 100–1150 cm^{-1}, shown in Figure 2, reveal further information on the structure of the films. Sample $mTiO_2$ yields four distinct Raman peaks at 146, 394, 516, and 637 cm^{-1} with slight broadening, as compared with the other two samples, which are directly attributable to the anatase phase [42]. This result is ascribed to the crystallinity of the anatase phase and is consistent with the XRD patterns. A shift in the high wave number and broad peak of the Raman spectrum at 146 cm^{-1} implies that the substitution of W ions into the MAO-anodized TiO_2 lattice and less well-crystallized TiO_2 particles probably occurred. The Raman peak at 810 cm^{-1} which is associated with the

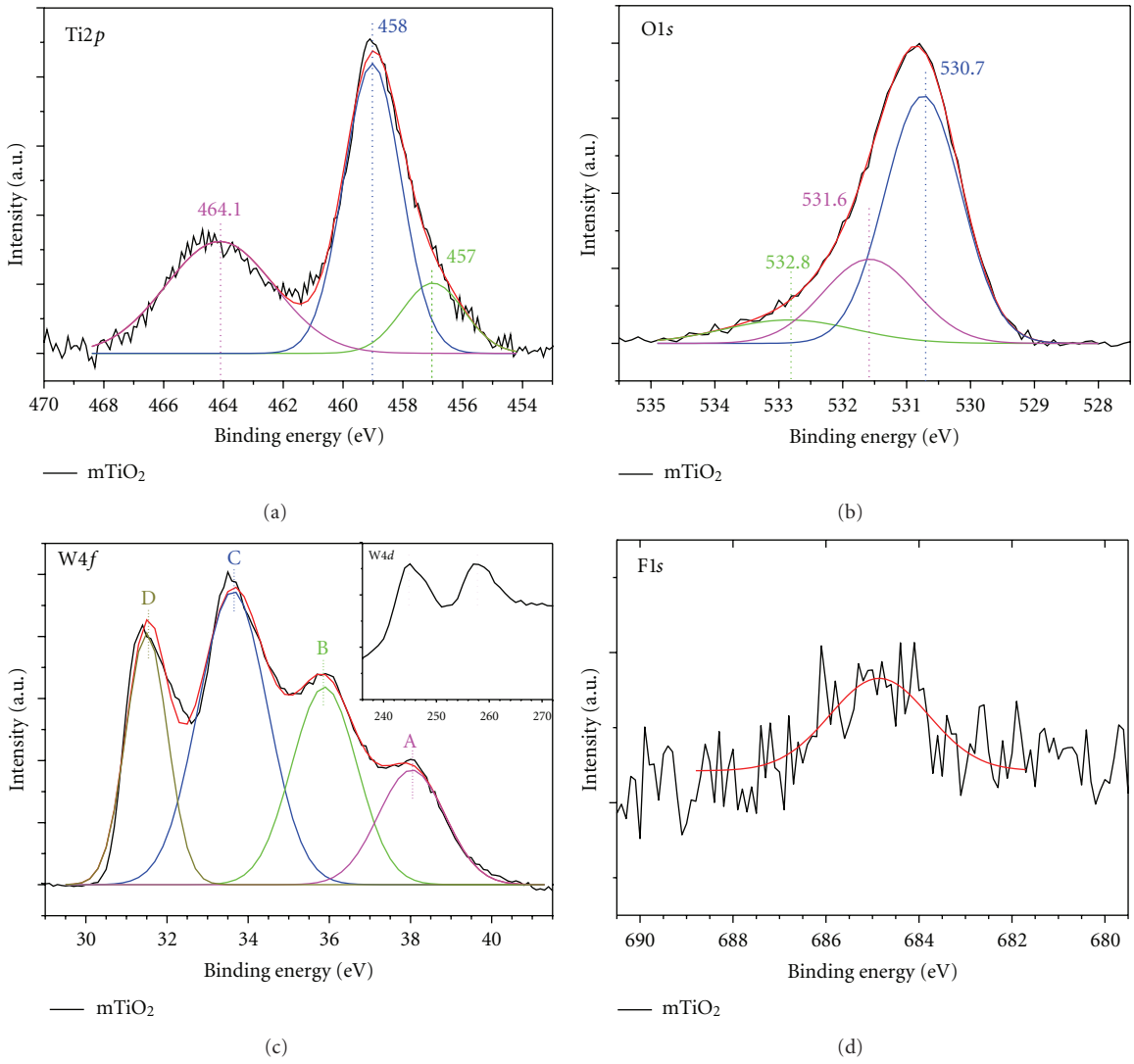

Figure 3: High resolution XPS spectrum of: (a) Ti2p, (b) O1s, (c) W4f/Wd, and (d) F1s core levels of the $mTiO_2$ film.

crystallized monoclinic or orthorhombic WO_3 is extremely weak, as shown in the inset of Figure 2, perhaps because of interference with a broad background signal of anatase TiO_2 [21]. A relatively broad band at 970 cm^{-1} is assigned to a terminal W=O stretching vibration in tungsten trioxide hydrates. Additionally, a shift in the high wave number of the WO_3 Raman spectrum at ~970 cm^{-1} reveals that WO_3 nanocrystallites had formed along the TiO_2 surface or grain boundaries in a relatively high W concentration [9, 16, 43], which was previously conformed by the EDS measurement.

3.2. XPS Analysis. High-resolution XPS measurements were performed to elucidate the surface chemical composition and the oxidation state for the porous $mTiO_2$ film. Curve fitting using Gaussian distribution function plotted in Figure 3(a), the XPS spectrum of Ti2p core level of the $mTiO_2$ film shows two well-known peaks at binding energy of ~459.0 eV and at ~464.1 eV, corresponding to $Ti2p_{3/2}$ and $Ti2p_{1/2}$, respectively, of Ti^{4+} oxidation state of TiO_2. A minor peak at binding energy of ~457.0 eV is also observed, which is assigned to Ti^{3+} of Ti_2O_3 phase and is in accordance with the XRD result presented in Figure 1. Alternatively, the O1s core level binding energies for sample $mTiO_2$ were deconvoluted into three distinct components, indicating that there are different kinds of O binding states in the $mTiO_2$ film, as shown in Figure 3(b). It is well stated that the peak at binding energy of 530.7 eV can be assigned as the crystal lattice oxygen of Ti–O and W–O binding, while the peaks at binding energy of 531.6 and 532.8 eV represent the oxygen in hydroxyl groups (O–H) and in adsorbed water molecules on the film [9, 37]. It is worthy to note that the area under hydroxyl groups (O–H) is estimated to be as large as 26.2%, which is ascribed for enhancing photocatalytic activity [44].

As seen in Figure 3(c), though the peak positions of $W4f_{5/2}$ (A) and $W4f_{7/2}$ (B) shift to a higher binding energy compared to the reported values, their oxidation state of the incorporated tungsten species is reportedly assigned as W^{+6} oxidation state of of pure WO_3 [9]. The lower binding energy

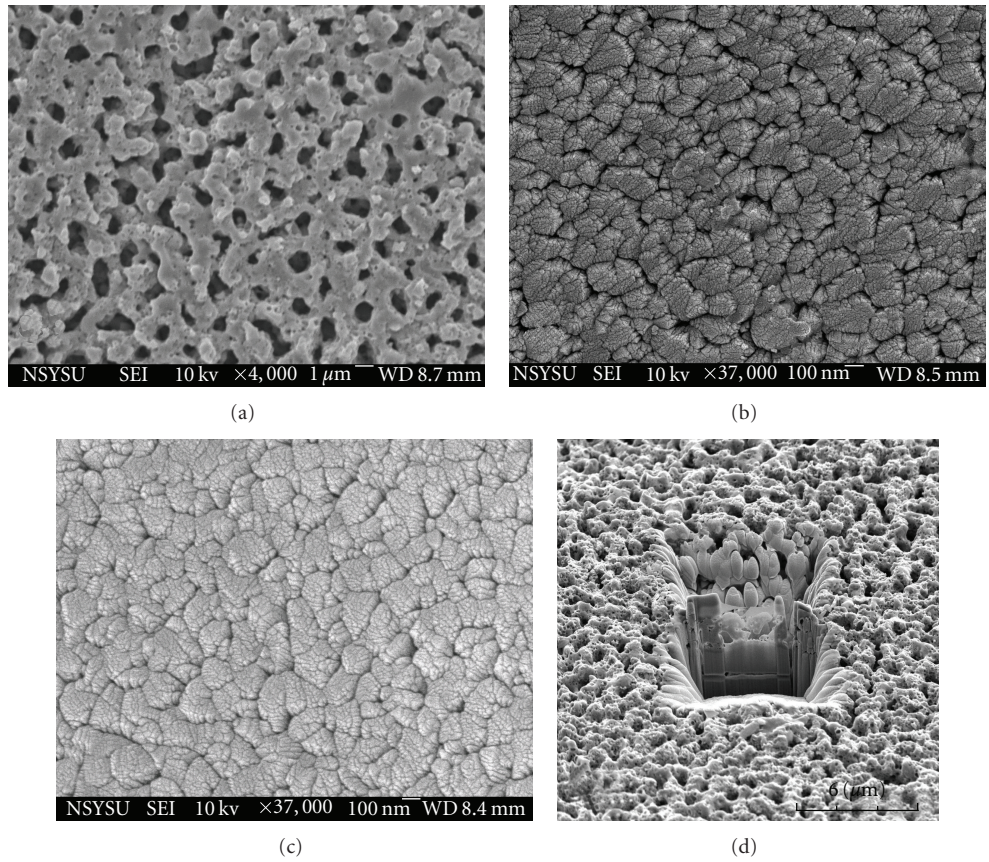

Figure 4: SEM plain images of (a) $mTiO_2$, (b) $nTiO_2$, and (c) $uTiO_2$ films and (d) FIB projected image of the $mTiO_2$ film, where the squared crater at the center was the TEM sample cut from.

shift can also be seen in the W4d peaks of sample $mTiO_2$, as shown in the inset of Figure 3(c). These indicate that sample $mTiO_2$ was loaded with a considerably high amount of WO_3 phase. The other two peaks (C and D) are intuitively assigned to other tungsten oxide (i.e., WO_2) or some nonstoichiometric tungsten oxides such as $W_{12}O_{39}{}^{n-}$ and impurities from the precursors used. Nevertheless, some other phases possibly form, since stoichiometric ion exchange between W^{4+} and Ti^{4+} may occur [17]. In fact, W^{4+} can substitute Ti^{4+} in the lattice of TiO_2 due to the similarity in their ion radii; nonstoichiometric solid solution of $W_xTi_{1-x}O_2$ forms. Thus, nonstoichiometric solid solution of $W_xTi_{1-x}O_2$ can form and leads to produce a tungsten impurity energy level [17]. Some researchers have reported that the W4f peaks of WO_3-loaded TiO_2 shift to a lower binding energy [43], but others have found a backward shift, as compared to that of pure WO_3 [37]. This may be due to different methods and precursors involved in sample preparation. This is being under taken further investigation in our lab. As seen in Figure 3(d), a weak and broad F1s peak at binding energy of ~684.9 eV is observed for sample $mTiO_2$, which is mostly originated from F^- ions physically adsorbed on the TiO_2 surface [24]. Park and Choi have conclude that the adsorbed F^- ions induce enhancement in the production of •OH radicals [44] when the F-containing compounds were used as TiO_2 precursors. However, no peak around 687.6 eV is observed which is attributed to the doped F atoms in TiO_2 [24, 45].

On the basis of the XPS results stated above, it can be briefly concluded that F^- ions is physically adsorbed on the TiO_2 surface in a very low concentration and W ions are likely loaded as a pure WO_3 phase along with other tungsten oxides and $W_xTi_{1-x}O_2$ composite on the $mTiO_2$ film.

3.3. Morphological and Topographical Observations. Porous TiO_2 films with improved connectivity are reportedly important for adsorbing organic contaminant ions or initiating various redox reactions [29]. Figure 4(a) presents the morphological SEM image of sample $mTiO_2$, showing a typical porous MAO structure with some submicron pores and colloidal particles on a large cavity. Moreover, Figure 4(d) shows a FIB projected image of the $mTiO_2$, where sponge-like morphology is filled with various micron and submicron pores. These submicron pores were probably formed by the secondary breakdown of the large pores that were produced by the primary breakdown of arcing [29]. The wall of the larger pores includes smaller pores and several pores inside the film of which increases its reactive site surface area. On the other hand, as shown in Figures 4(b) and 4(c), samples $nTiO_2$ and $uTiO_2$ exhibit a typical columnar-like morphologies deposited by a DC magnetron sputtering

Table 1: Some properties and apparent rate constants of three samples.

Sample	Band gap energy, eV	Specific surface area, m^2/g	Apparent rate constant, h^{-1}	
			UV	Vis
$mTiO_2$	2.23	1.75	0.53	0.42
$nTiO_2$	2.93	0.16*	0.33	0.28
$uTiO_2$	3.25	0.14*	0.36	0.06

* estimated from the AFM measurement [37].

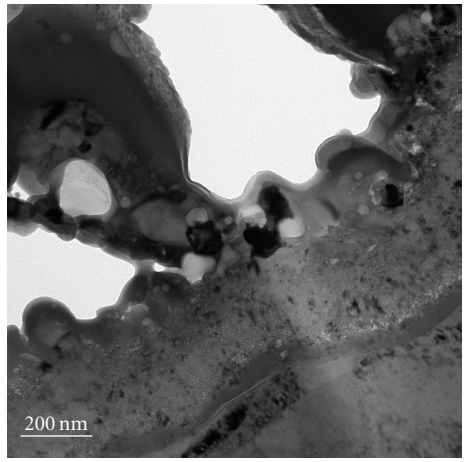

Figure 5: Cross-sectional TEM micrograph of the $mTiO_2$ film in which the porous TiO_2 was formed on a 300 nm-thick TiO_2 layer supported by Ti substrate.

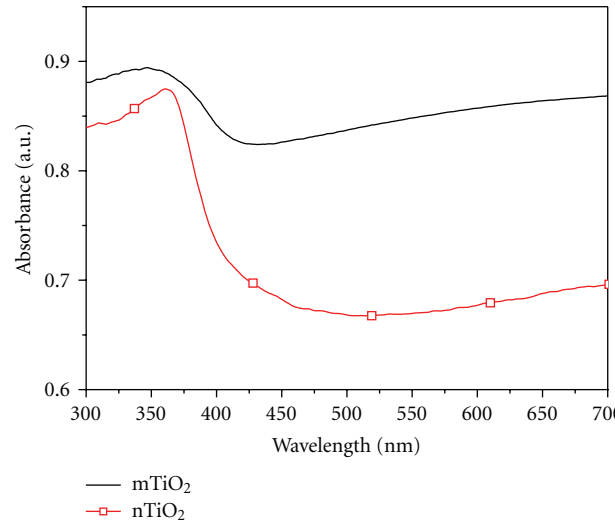

Figure 6: Diffused reflection spectra of the $mTiO_2$ and $nTiO_2$ films.

technique [15, 39]. Thus, a low specific surface area is expected, rendering a low active area in contact with aqueous solution. The cross-sectional TEM micrograph of the $mTiO_2$ film in Figure 5 reveals that a pore diameter ranging from 400 to 800 nm was formed on a WO_3/TiO_2 layer with a thickness of about 300 nm. The porous network connected by many micron pores is regarded as an open with randomly orientated channels in the porous film.

The specific roughness factor of $nTiO_2$ and $uTiO_2$ films (Figures 4(b) and 4(c)) were previously reported to be about 1.3 and 1.2, which were equal to surface areas of about 0.16 m^2/g and 0.14 m^2/g, respectively (Table 1) [15, 39]. The $mTiO_2$ shows a BET surface area of 1.75 m^2/g, which is ten times greater more than that of the $nTiO_2$ and $uTiO_2$. Thus, extremely rough, network-structured, and well-crystallized TiO_2 films can be obtained by MAO process without any subsequent heat treatment.

3.4. Optical Properties. Figure 6 shows the diffused reflection spectra of sample $mTiO_2$ film, displaying broad absorbance across the UV-Vis regions. Obviously, sample $mTiO_2$ has a better optical absorption in the region of 400–700 nm owing to the presence of tungsten oxides and solid solution of $W_xTi_{1-x}O_2$ than the N,C-TiO_2 and pure TiO_2 [17]. It is well known that the absorption edge of the samples shift toward the Vis region as WO_3 is loaded on TiO_2 matrix [9, 16–19, 37]. The band gap energies are calculated according to the equation $E_g = hc/\lambda$, where E_g is the band gap energy (eV), h is the Planck's constant (4.136×10^{-15} eV s), c is the velocity of light (2.99×10^8 m/s), and λ is the wavelength (nm) of absorption onset [36, 40]. The band gap energies are 2.23 eV for $mTiO_2$ and 2.93 eV for $nTiO_2$ films, whereas that is estimated to be 3.25 eV for the pure TiO_2 [39]. Although some researchers reported that only F-doping did not cause any significant change in the optical absorption of TiO_2 (2.90–2.95 eV [24, 26]), they observed a new absorption band in the visible range of 400–550 nm in addition to a strong fundamental absorption edge (~387 nm) of TiO_2 [24, 45]. Thus, the shift towards the longer wavelengths markedly originates from the band gap narrowing of TiO_2 by coupling with tungsten oxides [37, 43] and possibly a complex of $W_xTi_{1-x}O_2$ [17].

3.5. Photocatalytic Activities. PC activity can be increased by increasing the apparent reaction rate constant and the equilibrium adsorption constant of the catalysts [16]. Figure 7 plots the degraded concentration of the MB solution against the reaction time of three different samples. No significant MB degradation is observed in a blank substrate under UV radiation. As expected, Figure 7 clearly reveals that the adsorption of MB by sample $mTiO_2$ was stronger than that of samples $nTiO_2$ and $uTiO_2$, due to the cationic nature of MB dye [17]. The MB adsorption capacity of TiO_2/WO_3 composites usually increases with the loading

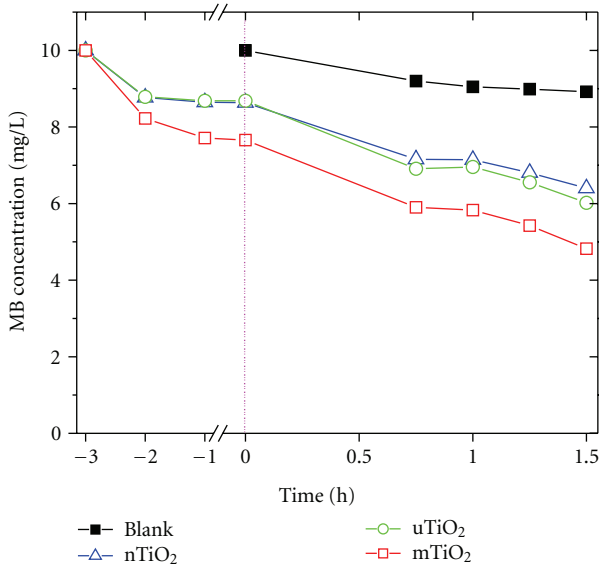

Figure 7: MB adsorption and degradation of the $mTiO_2$, $nTiO_2$, and $uTiO_2$ films under UV irradiation. Blank and absorption tests are presented for comparisons.

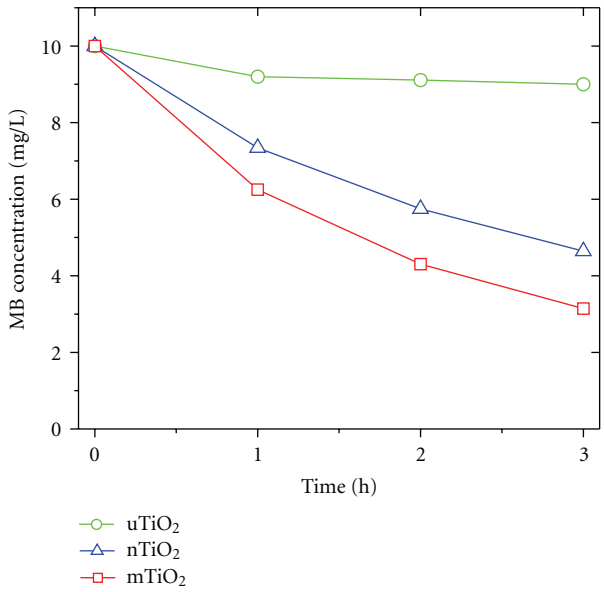

Figure 8: MB degradation of the $mTiO_2$, $nTiO_2$, and $uTiO_2$ films under BLED irradiation.

of WO_3 clusters [16, 20, 46], because the surface acidity of a WO_3 monolayer results in strong adsorption of the TiO_2/WO_3 composites [20]. This result implies that the enhanced MB adsorption capacity of sample $mTiO_2$ is probably associated with the specific surface area of the sample that were prepared by the MAO process other than by the formation of WO_3 clusters in the TiO_2/WO_3 composites, suggesting that the MB adsorption capacity is related not only to the surface acidity of the WO_3 clusters, but also to the specific roughness factor [20, 21, 46].

As listed in Table 1, under UV irradiation, sample $mTiO_2$ exhibits the highest activity of the three samples tested, showing the highest apparent rate constant of $0.53\,h^{-1}$–61% greater than that, $0.33\,h^{-1}$, of sample $nTiO_2$. Sample $mTiO_2$, broad absorbance observed in the Vis regions, exhibits significant PC activity under BLED irradiation, an apparent rate constant of $0.42\,h^{-1}$–50% greater than that, $0.28\,h^{-1}$, of sample $nTiO_2$, as shown in Figure 8. Sample $nTiO_2$ has an apparent rate constant of $0.36\,h^{-1}$ and $0.06\,h^{-1}$ under UV and Vis irradiation, respectively.

The PC activity of TiO_2 depends on several factors, including crystallinity [47], surface area [8], crystal orientation [48], surface hydroxyl density, and phase composition [49, 50]. In general, the photogenerated charge carrier transfer to the film surface would be limited by the interfacial diffusion between crystalline WO_3/TiO_2 particles, which is faster than volume diffusion. And the sponge-like porous structure of the $mTiO_2$ film can make charge carrier easier to reach the surface than a typical planar $nTiO_2$ sample. The porous $mTiO_2$ film exhibits the highest PC activity among the oxides of interest; surprisingly, only 50%–61% higher in photocatalytic activity obtained from the film with ten times greater more in the surface area than others. Qualitatively, the $mTiO_2$ film consists of TiO_2 and WO_3 crystallites with a higher specific surface area and a lower crystallinity than the $nTiO_2$ and $uTiO_2$ films. The PC activity of $mTiO_2$ is enhanced by its WO_3 crystallites and high specific surface area but is reduced by its low crystallinity and some impurities, such as Ti and Na elements. Impurities act as carrier recombination centers in an oxide and always detrimentally affect PC activity. In contrast, high crystallinity is associated with a small fraction of crystal defects that act as recombination sites [7–9], allowing the generated charges to diffuse to the crystallite surface without undergoing recombination [4]. Thus, improvement of crystallinity is a possible way to increase the film photocatalytic ability.

In addition, though WO_3 has a conduction band that allows for the transfer of photogenerated electrons from TiO_2, its valence band is not positioned properly toward to the coupled TiO_2; therefore, effective charge separation cannot be fully obtained in crystalline TiO_2/WO_3 heterostructures [41]. The formation of WO_3 crystallites, randomly distributed along TiO_2 nanocrystals, rather than the highly adsorbing WO_3 monolayer or amorphous WO_x, reduces the adsorption capacity of WO_3 [20, 41]. Finally, the amount of tungsten loaded onto TiO_2 was not optimized herein, but this factor reportedly is important in determining PC activity [9, 16, 21, 46].

4. Conclusions

In this study, a porous F-TiO_2/WO_3 film with crystallized anatase TiO_2 phase and network-framed structure was successfully obtained by microarc oxidation without subsequent heat treatment. The F-TiO_2/WO_3 film exhibits high photocatalytic activity in MB degradation under UV and BLED irradiation. The Vis PC efficiency is dominated by the incorporation of tungsten oxides and possibly a complex of $W_xTi_{1-x}O_2$. The specific surface area of the film

is one of the most important parameters in determining the efficiency of the PC process, because a higher specific surface area favors the adsorption of more MB molecules on its active sites. Thus, the elucidated MAO process is one of the most cost-effective methods for producing films in practical photocatalytic applications.

Acknowledgment

The authors would like to thank the National Science Council of the Republic of China, Taiwan, for financially supporting this research under Contract No. NSC 98-2221-E-022-004-MY2.

References

[1] A. Fujishima, T. N. Rao, and D. A. Tryk, "Titanium dioxide photocatalysis," *Journal of Photochemistry and Photobiology C*, vol. 1, no. 1, pp. 1–21, 2000.

[2] Y. Ma, J. B. Qiu, Y. A. Cao, Z. S. Guan, and J. N. Yao, "Photocatalytic activity of TiO_2 films grown on different substrates," *Chemosphere*, vol. 44, no. 5, pp. 1087–1092, 2001.

[3] M. Radecka, M. Rekas, A. Trenczek-Zajac, and K. Zakrzewska, "Importance of the band gap energy and flat band potential for application of modified TiO_2 photoanodes in water photolysis," *Journal of Power Sources*, vol. 181, no. 1, pp. 46–55, 2008.

[4] N. Masahashi, Y. Mizukoshi, S. Semboshi, and N. Ohtsu, "Enhanced photocatalytic activity of rutile TiO_2 prepared by anodic oxidation in a high concentration sulfuric acid electrolyte," *Applied Catalysis B*, vol. 90, no. 1-2, pp. 255–261, 2009.

[5] D. Gong, C. A. Grimes, O. K. Varghese et al., "Titanium oxide nanotube arrays prepared by anodic oxidation," *Journal of Materials Research*, vol. 16, no. 12, pp. 3331–3334, 2001.

[6] Z. Liu, X. Zhang, S. Nishimoto et al., "Highly ordered TiO_2 nanotube arrays with controllable length for photoelectrocatalytic degradation of phenol," *Journal of Physical Chemistry C*, vol. 112, no. 1, pp. 253–259, 2008.

[7] Y. Liu, B. Zhou, J. Bai et al., "Efficient photochemical water splitting and organic pollutant degradation by highly ordered TiO_2 nanopore arrays," *Applied Catalysis B*, vol. 89, no. 1-2, pp. 142–148, 2009.

[8] J. Ryu, D. S. Park, B. D. Hahn et al., "Photocatalytic TiO_2 thin films by aerosol-deposition: from micron-sized particles to nano-grained thin film at room temperature," *Applied Catalysis B*, vol. 83, no. 1-2, pp. 1–7, 2008.

[9] J. H. Pan and W. I. Lee, "Preparation of highly ordered cubic mesoporous WO_3/TiO_2 films and their photocatalytic properties," *Chemistry of Materials*, vol. 18, no. 3, pp. 847–853, 2006.

[10] Y. Zhao, X. Zhang, J. Zhai et al., "Enhanced photocatalytic activity of hierarchically micro-/nano-porous TiO_2 films," *Applied Catalysis B*, vol. 83, no. 1-2, pp. 24–29, 2008.

[11] H. Irie, H. Mori, and K. Hashimoto, "Interfacial structure dependence of layered TiO_2/WO_3 thin films on the photo-induced hydrophilic property," *Vacuum*, vol. 74, no. 3-4, pp. 625–629, 2004.

[12] W. Dai, X. Wang, P. Liu, Y. Xu, G. Li, and X. Fu, "Effects of electron transfer between TiO_2 films and conducting substrates on the photocatalytic oxidation of organic pollutants," *Journal of Physical Chemistry B*, vol. 110, no. 27, pp. 13470–13476, 2006.

[13] H. Chen, S. Chen, X. Quan, H. Yu, H. Zhao, and Y. Zhang, "Fabrication of TiO_2-Pt coaxial nanotube array Schottky structures for enhanced photocatalytic degradation of phenol in aqueous solution," *Journal of Physical Chemistry C*, vol. 112, no. 25, pp. 9285–9290, 2008.

[14] J. Bai, J. Li, Y. Liu, B. Zhou, and W. Cai, "A new glass substrate photoelectrocatalytic electrode for efficient visible-light hydrogen production: CdS sensitized TiO_2 nanotube arrays," *Applied Catalysis B*, vol. 95, no. 3-4, pp. 408–413, 2010.

[15] K. R. Wu, C. H. Hung, and M. H. Tsai, "Effects of ITO thin films on microstructural and photocatalytic properties of layered TiO_2/ITO films prepared via an extended deposition period," *Applied Catalysis B*, vol. 92, no. 3-4, pp. 357–366, 2009.

[16] K. K. Akurati, A. Vital, J. P. Dellemann et al., "Flame-made WO_3/TiO_2 nanoparticles: relation between surface acidity, structure and photocatalytic activity," *Applied Catalysis B*, vol. 79, no. 1, pp. 53–62, 2008.

[17] X. Z. Li, F. B. Li, C. L. Yang, and W. K. Ge, "Photocatalytic activity of WO_x-TiO_2 under visible light irradiation," *Journal of Photochemistry and Photobiology A*, vol. 141, no. 2-3, pp. 209–217, 2001.

[18] Y. Lu, M. Yuan, Y. Liu et al., "Photoelectric performance of bacteria photosynthetic proteins entrapped on tailored mesoporous WO_3-TiO_2 films," *Langmuir*, vol. 21, no. 9, pp. 4071–4076, 2005.

[19] T. Tatsuma, S. Saitoh, Y. Ohko, and A. Fujishima, "TiO_2-WO_3 photoelectrochemical anticorrosion system with an energy storage ability," *Chemistry of Materials*, vol. 13, no. 9, pp. 2838–2842, 2001.

[20] Y. T. Kwon, K. Y. Song, W. I. Lee, G. J. Choi, and Y. R. Do, "Photocatalytic behavior of WO_3-loaded TiO_2 in an oxidation reaction," *Journal of Catalysis*, vol. 191, no. 1, pp. 192–199, 2000.

[21] O. Lorret, D. Francová, G. Waldner, and N. Stelzer, "W-doped titania nanoparticles for UV and visible-light photocatalytic reactions," *Applied Catalysis B*, vol. 91, no. 1-2, pp. 39–46, 2009.

[22] D. Li, H. Haneda, S. Hishita, and N. Ohashi, "Visible-light-driven N-F-codoped TiO_2 photocatalysts. 1. Synthesis by spray pyrolysis and surface characterization," *Chemistry of Materials*, vol. 17, no. 10, pp. 2588–2595, 2005.

[23] G. Wu and A. Chen, "Direct growth of F-doped TiO_2 particulate thin films with high photocatalytic activity for environmental applications," *Journal of Photochemistry and Photobiology A*, vol. 195, no. 1, pp. 47–53, 2008.

[24] J. C. Yu, J. Yu, W. Ho, Z. Jiang, and L. Zhang, "Effects of F-doping on the photocatalytic activity and microstructures of nanocrystalline TiO_2 powders," *Chemistry of Materials*, vol. 14, no. 9, pp. 3808–3816, 2002.

[25] N. Serpone, "Is the band gap of pristine TiO_2 narrowed by anion- and cation-doping of titanium dioxide in second-generation photocatalysts?" *Journal of Physical Chemistry B*, vol. 110, no. 48, pp. 24287–24293, 2006.

[26] J. F. Li, L. Wan, and J. Y. Feng, "Study on the preparation of titania films for photocatalytic application by micro-arc oxidation," *Solar Energy Materials and Solar Cells*, vol. 90, no. 15, pp. 2449–2455, 2006.

[27] J. He, Q. Z. Cai, Y. G. Ji, H. H. Luo, D. J. Li, and B. Yu, "Influence of fluorine on the structure and photocatalytic activity of TiO_2 film prepared in tungstate-electrolyte via micro-arc oxidation," *Journal of Alloys and Compounds*, vol. 482, no. 1-2, pp. 476–481, 2009.

[28] W. Xiaohong, Q. Wei, D. Xianbo, H. Weidong, and J. Zhaohua, "Dopant influence on the photo-catalytic activity of TiO_2 films prepared by micro-plasma oxidation method," *Journal of Molecular Catalysis A*, vol. 268, no. 1-2, pp. 257–263, 2007.

[29] J. Li, L. Wan, and J. Feng, "Micro arc oxidation of S-containing TiO_2 films by sulfur bearing electrolytes," *Journal of Materials Processing Technology*, vol. 209, no. 2, pp. 762–766, 2009.

[30] Y. Wang, L. Wang, H. Zheng et al., "Effect of frequency on the structure and cell response of Ca- and P-containing MAO films," *Applied Surface Science*, vol. 256, no. 7, pp. 2018–2024, 2010.

[31] D. Wei, Y. Zhou, D. Jia, and Y. Wang, "Characteristic and in vitro bioactivity of a microarc-oxidized TiO_2-based coating after chemical treatment," *Acta Biomaterialia*, vol. 3, no. 5, pp. 817–827, 2007.

[32] L. H. Li, Y. M. Kong, H. W. Kim et al., "Improved biological performance of Ti implants due to surface modification by micro-arc oxidation," *Biomaterials*, vol. 25, no. 14, pp. 2867–2875, 2004.

[33] H. T. Chen, C. H. Hsiao, H. Y. Long et al., "Micro-arc oxidation of β-titanium alloy: structural characterization and osteoblast compatibility," *Surface and Coatings Technology*, vol. 204, no. 6-7, pp. 1126–1131, 2009.

[34] F. Deng, W. Zhang, P. Zhang, C. Liu, and J. Ling, "Improvement in the morphology of micro-arc oxidised titanium surfaces: a new process to increase osteoblast response," *Materials Science and Engineering C*, vol. 30, no. 1, pp. 141–147, 2010.

[35] R. H. U. Khan, A. L. Yerokhin, and A. Matthews, "Structural characteristics and residual stresses in oxide films produced on Ti by pulsed unipolar plasma electrolytic oxidation," *Philosophical Magazine*, vol. 88, no. 6, pp. 795–807, 2008.

[36] J. He, Q. Z. Cai, Q. Luo, D. Q. Zhang, T. T. Tang, and Y. F. Jiang, "Photocatalytic removal of methyl orange in an aqueous solution by a WO_3/TiO_2 composite film," *Korean Journal of Chemical Engineering*, vol. 27, no. 2, pp. 435–438, 2010.

[37] M. R. Bayati, F. Golestani-Fard, and A. Z. Moshfegh, "Visible photodecomposition of methylene blue over micro arc oxidized WO_3-loaded TiO_2 nano-porous layers," *Applied Catalysis A*, vol. 382, no. 2, pp. 322–331, 2010.

[38] S. Y. Wu, W. C. Lo, K. C. Chen, and J. L. He, "Study on the preparation of nano-flaky anatase titania layer and their photovoltaic application," *Current Applied Physics*, vol. 10, no. 2, pp. S180–S183, 2010.

[39] K. R. Wu and C. H. Hung, "Characterization of N,C-codoped TiO_2 films prepared by reactive DC magnetron sputtering," *Applied Surface Science*, vol. 256, no. 5, pp. 1595–1603, 2009.

[40] X. Yang, C. Cao, L. Erickson, K. Hohn, R. Maghirang, and K. Klabunde, "Synthesis of visible-light-active TiO_2-based photocatalysts by carbon and nitrogen doping," *Journal of Catalysis*, vol. 260, no. 1, pp. 128–133, 2008.

[41] S. Higashimoto, M. Sakiyama, and M. Azuma, "Photoelectrochemical properties of hybrid WO_3/TiO_2 electrode. Effect of structures of WO_3 on charge separation behavior," *Thin Solid Films*, vol. 503, no. 1-2, pp. 201–206, 2006.

[42] V. Swamy, A. Kuznetsov, L. S. Dubrovinsky, R. A. Caruso, D. G. Shchukin, and B. C. Muddle, "Finite-size and pressure effects on the Raman spectrum of nanocrystalline anatase Ti O2," *Physical Review B*, vol. 71, no. 18, Article ID 184302, 2005.

[43] B. Gao, Y. Ma, Y. Cao, W. Yang, and J. Yao, "Great enhancement of photocatalytic activity of nitrogen-doped titania by coupling with tungsten oxide," *Journal of Physical Chemistry B*, vol. 110, no. 29, pp. 14391–14397, 2006.

[44] J. S. Park and W. Choi, "Enhanced remote photocatalytic oxidation on surface-fluorinated TiO_2," *Langmuir*, vol. 20, no. 26, pp. 11523–11527, 2004.

[45] D. Li, H. Haneda, S. Hishita, and N. Ohashi, "Visible-light-driven N-F-codoped TiO_2 photocatalysts. 2. Optical characterization, photocatalysis, and potential application to air purification," *Chemistry of Materials*, vol. 17, no. 10, pp. 2596–2602, 2005.

[46] Saepurahman, M. A. Abdullah, and F. K. Chong, "Dual-effects of adsorption and photodegradation of methylene blue by tungsten-loaded titanium dioxide-1," *Chemical Engineering Journal*, vol. 158, pp. 418–425, 2010.

[47] M. Inagaki, R. Nonaka, B. Tryba, and A. W. Morawski, "Dependence of photocatalytic activity of anatase powders on their crystallinity," *Chemosphere*, vol. 64, no. 3, pp. 437–445, 2006.

[48] H. G. Yang, C. H. Sun, S. Z. Qiao et al., "Anatase TiO_2 single crystals with a large percentage of reactive facets," *Nature*, vol. 453, no. 7195, pp. 638–641, 2008.

[49] A. Brudnik, A. Gorzkowska-Sobaś, E. Pamuła, M. Radecka, and K. Zakrzewska, "Thin film TiO_2 photoanodes for water photolysis prepared by dc magnetron sputtering," *Journal of Power Sources*, vol. 173, no. 2, pp. 774–780, 2007.

[50] M. Toyoda, Y. Nanbu, Y. Nakazawa, M. Hirano, and M. Inagaki, "Effect of crystallinity of anatase on photoactivity for methyleneblue decomposition in water," *Applied Catalysis B*, vol. 49, no. 4, pp. 227–232, 2004.